Geophysical Research Letters

RESEARCH LETTER
10.1002/2018GL077622

Special Section:
Impact of the Sept. 10, 2017, Solar Event on Mars

MARSIS Observations of the Martian Nightside Ionosphere During the September 2017 Solar Event

Y. Harada[1,2], D. A. Gurnett[1], A. J. Kopf[1], J. S. Halekas[1], S. Ruhunusiri[1], G. A. DiBraccio[3], J. Espley[2], and D. A. Brain[4]

[1]Department of Physics and Astronomy, University of Iowa, Iowa City, IA, USA, [2]Department of Geophysics, Kyoto University, Kyoto, Japan, [3]NASA Goddard Space Flight Center, Greenbelt, MD, USA, [4]Laboratory for Atmospheric and Space Physics, University of Colorado Boulder, Boulder, CO, USA

Key Points:
- MARSIS on the nightside and MAVEN on the dayside observed the global response of the Martian ionosphere to the September 2017 solar event
- Nightside peak electron densities and global ionospheric magnetic fields exhibited unusually high values during the event
- Electron impact ionization is a likely source for the nightside peak electron density enhancement around 120 km altitudes

Correspondence to:
Y. Harada,
yuki-harada@uiowa.edu

Citation:
Harada, Y., Gurnett, D. A., Kopf, A. J., Halekas, J. S., Ruhunusiri, S., DiBraccio, G. A., et al. (2018). MARSIS observations of the Martian nightside ionosphere during the September 2017 solar event. *Geophysical Research Letters*, *45*, 7960–7967. https://doi.org/10.1002/2018GL077622

Received 20 FEB 2018
Accepted 2 MAR 2018
Accepted article online 6 MAR 2018
Published online 19 AUG 2018

Abstract We present topside ionospheric sounding on the nightside of Mars during the September 2017 solar event by Mars Advanced Radar for Subsurface and Ionosphere Sounding (MARSIS) on board Mars Express along with complementary dayside observations from Mars Atmosphere and Volatile EvolutioN (MAVEN). The MARSIS and MAVEN observations during the event suggest that (i) the nightside bottomside ionosphere was significantly enhanced by solar energetic particles, (ii) the nightside peak electron density was increased to unusually high values of $\sim 1-2 \times 10^4$ cm^{-3} around 120 km altitudes owing to enhanced electron impact ionization, and (iii) the ionospheric magnetic field was globally amplified by the high dynamic pressure during the interplanetary coronal mass ejection passage. These multipoint measurements help elucidate the global response of the Martian upper ionosphere to the solar event.

Plain Language Summary The solar flare that occurred on 10 September 2017, and the subsequent coronal mass ejection had major impacts on the upper atmosphere of Mars. In this work, we study how the Martian ionosphere, which is the ionized part of the upper atmosphere, changed in response to this prominent solar event. Analysis of data from two spacecraft, Mars Express and MAVEN, reveals unusually strong magnetic fields everywhere in the ionosphere and an exceptionally high level of ionization during the night time. These results can be compared and combined with other observations and models and help the ongoing community wide effort to understand the effects of the solar event on planetary environments.

1. Introduction

A solar flare that occurred on 10 September 2017, and the following solar energetic particles and interplanetary coronal mass ejection (ICME) caused a variety of observed effects on the upper atmosphere of Mars (see Lee et al., 2018, and other papers in this issue for a detailed timeline of the solar event and observed and modeled responses of Mars). This paper reports on the response of the nightside ionosphere of Mars to the September 2017 solar event as observed by the Mars Advanced Radar for Subsurface and Ionosphere Sounding (MARSIS) instrument on board Mars Express. MARSIS conducts ionospheric sounding by transmitting a short electromagnetic pulse and measuring an echo reflected from the topside ionosphere. MARSIS ionospheric measurements can be utilized to derive vertical electron density profiles of the topside ionosphere as well as the local electron density and magnetic field strength (Gurnett et al., 2008; Jordan et al., 2009). During the September 2017 solar event, the periapsis of Mars Express was located on the nightside, and MARSIS obtained remote and local information on the nightside ionosphere around the periapsis. As the Mars Atmosphere and Volatile EvolutioN (MAVEN) spacecraft sampled the dayside ionosphere near its periapsis during this event, MARSIS observations of the nightside ionosphere provide complementary information that is necessary if we are to characterize the global response of the upper atmosphere of Mars to the solar event. Furthermore, the derived quantities presented in this paper, such as electron density profiles and local magnetic field strengths, provide valuable data points in the nightside ionosphere which can be compared to results from the ongoing modeling effort to reproduce the evolution of the Martian system during this solar event.

2. Observations

We first present contextual information on the solar event from the extreme ultraviolet monitor (EUVM) (Eparvier et al., 2015), solar energetic particle (SEP) (Larson et al., 2015), solar wind ion analyzer (SWIA) (Halekas et al., 2015), Solar Wind Electron Analyzer (SWEA) (Mitchell et al., 2016), and magnetometer (MAG) (Connerney et al., 2015) instruments on board MAVEN. Figures 1a–1e show solar extreme ultraviolet and particle data obtained by MAVEN from 7 to 14 September 2017. The solar flare on 10 September 2017 (Figure 1a) was followed immediately by the intense fluxes of solar energetic particles (Figures 1b and 1c) and subsequently by the enhanced suprathermal particle fluxes associated with the ICME arrival on 13 September 2017 (Figures 1d and 1e). Figure 1f shows the magnitude of the induced magnetic field (obtained by subtracting the predicted crustal magnetic field (Morschhauser et al., 2014) from the measured field) below 1,000 km altitudes at solar zenith angles (SZA) of ∼66–74°, displaying the ionospheric magnetic field enhancement correlated with the increased flux of suprathermal particles. The red bars in Figure 1g indicate the times when MARSIS operated in the Active Ionospheric Sounder mode. Of the three segments of MARSIS Active Ionospheric Sounder operation seen in Figure 1g, two orbits provide periapsis measurements of the Martian ionosphere with one orbit well before the solar event (labeled "Quiet Orbit") and the other during the intense particle flux event ("Event Orbit").

Figure 2 shows the orbit geometry of Mars Express for the Quiet and Event orbits in Mars Solar Orbital and geographic coordinates along with MAVEN orbits in Mars Solar Orbital coordinates for reference. For both orbits, the MEX periapsis is located on the deep nightside (Figures 2a and 2b). As shown in Figures 2c and 2d, Mars Express was located above the equatorial region with moderate crustal fields at the beginning of the segments, traveled over the mostly unmagnetized region around the periapsis, and ended up in the strong crustal field region in the southern hemisphere. By analyzing MARSIS data from these two orbits, we can compare the state of the nightside ionosphere before and during the solar event at nearly identical spatial locations.

Figures 3a–3h present MARSIS data obtained during the Quiet orbit, providing a baseline of the nominal nightside ionosphere. Figures 3a and 3b show radargrams (echo intensities as a function of apparent altitude, $H' = c\Delta t/2$, where c is the speed of light and Δt is the time delay, and time) of ∼2 MHz and ∼1 MHz echoes, respectively. On the deep nightside at SZA >120° (Figure 3h), we observe the horizontal lines at the apparent altitude of 0 km (labeled "ground reflection" in Figure 3a), representing radio waves penetrating the tenuous nightside ionosphere and reflected from the surface of Mars. The absence of ionospheric echoes at these frequencies is a typical feature of the nightside ionosphere (e.g., Němec et al., 2010). As the spacecraft approached the terminator, hyperbola-shaped ionospheric traces were detected at apparent altitudes of ∼100 km ("oblique echo" in Figure 3b) above the strong and radial crustal fields (Figure 3c). These oblique echoes represent ionospheric echoes reflected obliquely from a fixed target associated with ionospheric structure formed near radial crustal magnetic fields (e.g., Gurnett et al., 2005). Figure 3d presents MARSIS data in another format, a spectrogram, showing echo intensities as a function of frequency and time, averaged over apparent altitudes between 20 km < H' < 150 km. The evenly spaced multiple lines represent "plasma oscillation harmonics," from which the local electron density can be inferred (e.g., Duru et al., 2008, 2011). The weak signals between 0.5 and 1.0 MHz were occasionally detected, representing echoes from the nightside ionosphere ("ionospheric echo"). The magenta lines in Figures 3d and 3e show the maximum frequencies of these ionospheric echoes manually selected from individual ionograms (snapshots of echo intensity as a function of time delay and frequency). The detected maximum frequencies and the absence of ionospheric echoes for a significant fraction of the time suggest that the peak electron density of the nominal nightside ionosphere mostly remains well below 10^4 cm^{-3} (the dashed line in Figure 3e), which is consistent with the previous study of Němec et al. (2010). In addition to the remote measurements, MARSIS provides in situ measurements of the local electron density (Figure 3f) derived from the plasma oscillation harmonics and the local magnetic field strength (Figure 3g) inferred from electron cyclotron echoes (Akalin et al., 2010; Gurnett et al., 2008). The local electron density measurements demonstrate the variable nature of the high-altitude nightside ionosphere with densities below ∼100 cm^{-3} (Figure 3f). Meanwhile, MARSIS detected local magnetic field strengths slightly above the crustal field strengths (Figure 3g), suggesting weak induced (noncrustal) fields of <∼ 10 nT. The MARSIS observations during the Quiet orbit exhibit typical nightside signatures including (i) clear ground traces, (ii) peak electron densities of <10^4 cm^{-3}, (iii) variable electron densities of <∼ 100 cm^{-3} at high altitudes above 300 km, and (iv) induced magnetic fields of <∼ 10 nT.

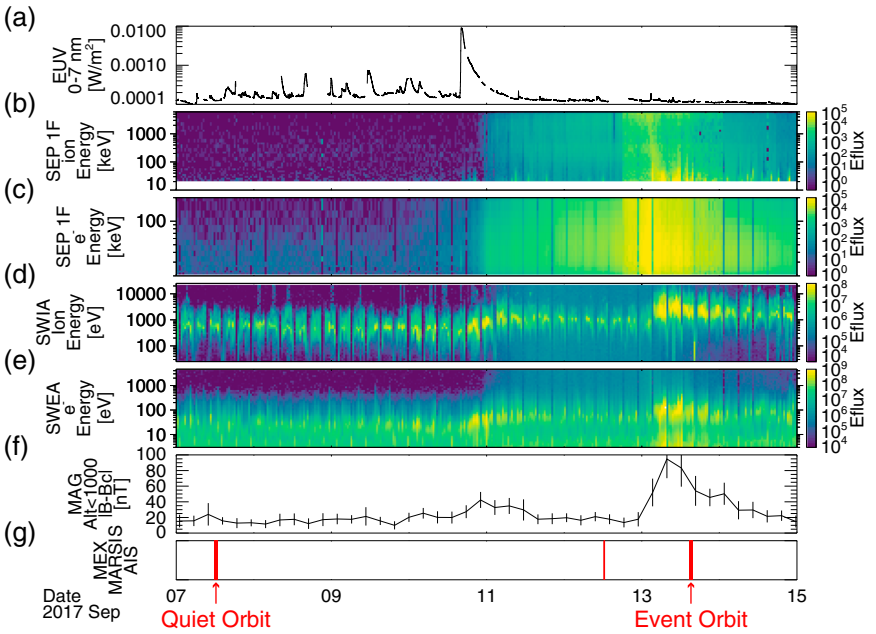

Figure 1. Mars Atmosphere and Volatile EvolutioN observations of (a) solar extreme ultraviolet (EUV) flux from the extreme ultraviolet monitor, and energy spectra in units of differential energy flux (Eflux) of eV/(cm^2 · s · sr · eV) of (b) energetic ions from SEP 1-Forward (1F) field of view, (c) energetic electrons from SEP 1F, (d) solar wind ions from Solar Wind Ion Analyzer (SWIA), (e) suprathermal electrons from Solar Wind Electron Analyzer (SWEA), and (f) magnitude of the induced magnetic field below 1,000 km altitude from magnetometer (MAG) on 7–14 September 2017. The red bars in Figure 1g show the availability of Mars Advanced Radar for Subsurface and Ionosphere Sounding (MARSIS) ionospheric data. MEX = Mars Express.

MARSIS measurements of the nightside ionosphere during the Event orbit are shown in Figures 3i–3p. In contrast to the clear ground trace seen during the Quiet orbit (Figures 3a and 3b), no ground reflection was detected during the Event orbit (Figure 3i). The disappearance of ground reflection is a well documented phenomenon often observed in association with high fluxes of solar energetic particles, and it is attributed

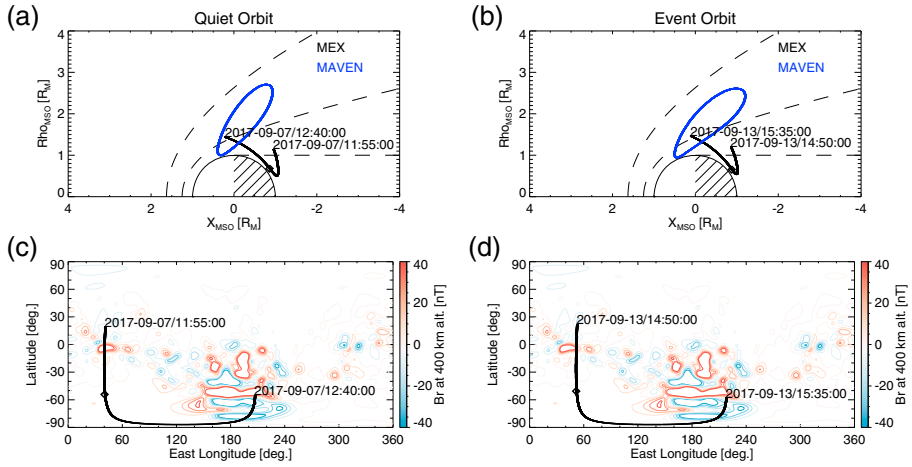

Figure 2. Orbit geometry of Mars Express for the "Quiet" and "Event" orbits (denoted in Figure 1) in (a and b) cylindrical Mars Solar Orbital and (c–d) geographic coordinates. The diamonds on the orbit tracks represent the periapsis locations. The dashed lines in Figures 2a and 2b denote the nominal positions of the bow shock and magnetic pileup boundary (MPB) (Trotignon et al., 2006) as well as the geometric shadow boundary. Mars Atmosphere and Volatile EvolutioN (MAVEN) orbit configurations are also shown for reference by the blue lines in Figures 2a and 2b. The contours in Figures 2c and 2d show the radial component of crustal magnetic fields at 400 km altitude computed from the spherical harmonic model (Morschhauser et al., 2014). MEX = Mars Express.

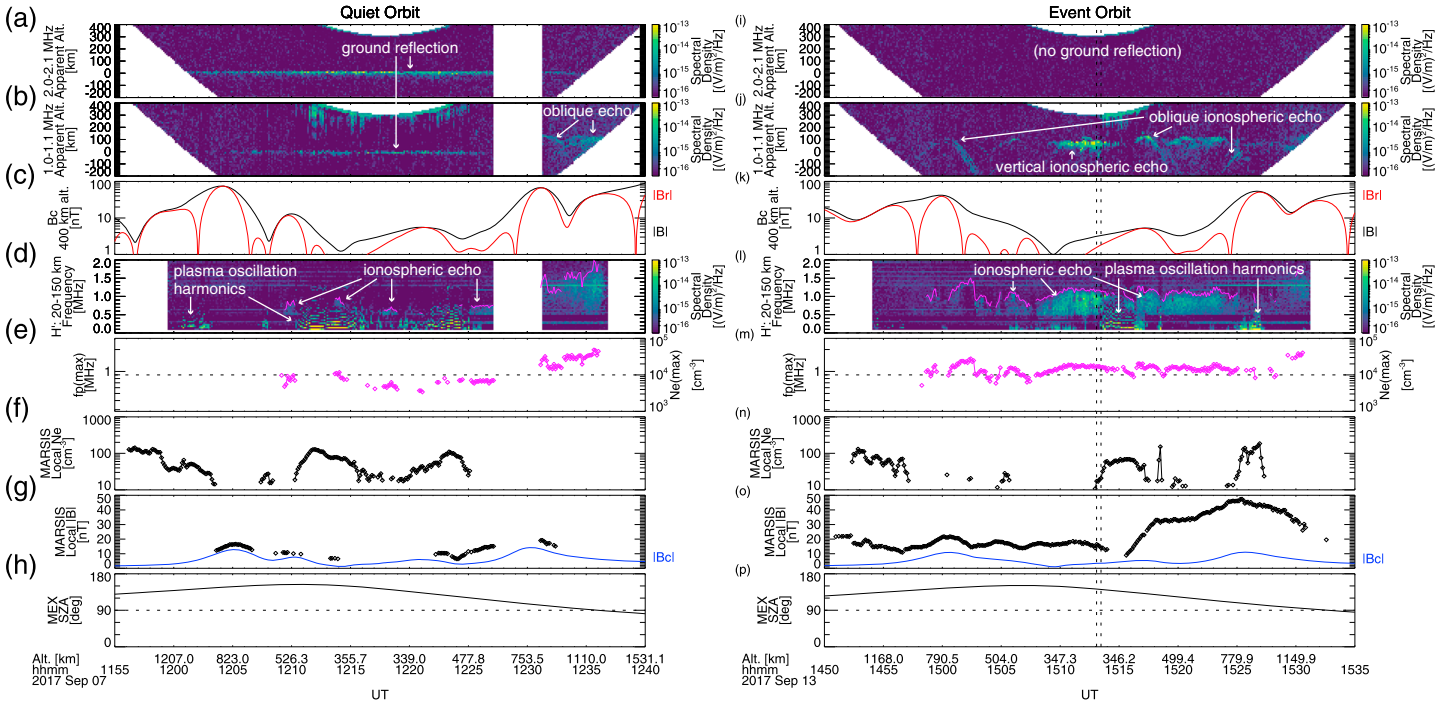

Figure 3. Mars Advanced Radar for Subsurface and Ionosphere Sounding (MARSIS) observations of radargrams of (a) 2.0–2.1 MHz echoes and (b) 1.0–1.1 MHz echoes, (c) crustal magnetic field strength (black) and magnitude of the radial component (red) at a 400 km altitude at the spacecraft longitude and latitude, (d) spectrogram (echo intensities as a function of frequency and time) with apparent altitudes of 20–150 km, (e) maximum frequency of detected ionospheric echoes and corresponding electron density (right axis), (f) local electron density, (g) local magnetic field strength and predicted crustal magnetic field strength (blue), and (h) solar zenith angle during the Quiet orbit and (i–p) those during the Event orbit. The spacecraft altitude is indicated in the text label. The magenta lines in Figures 3d and 3l represent the maximum ionospheric echo frequency shown in Figures 3e and 3m. The crustal magnetic fields are computed from the spherical harmonic model (Morschhauser et al., 2014). MEX = Mars Express

to radio wave attenuation by enhanced ionization mainly at low altitudes below 100 km (Espley et al., 2007; Morgan et al., 2006, 2010, 2014; Němec et al., 2014, 2015, 2007). At 1 MHz (Figure 3j), we observe oblique ionospheric echoes above radial crustal fields as well as vertical ionospheric echoes near the periapsis at SZA ~140° (the horizontal trace labeled as "vertical ionospheric echo" in Figure 3j, representing echoes reflected vertically from the horizontally stratified ionosphere). The peak densities inferred from these ionospheric echoes exceed 10^4 cm^{-3} for most of the time (Figures 3l and 3m). These peak densities are unusually high for the nightside ionosphere, given that the nightside peak electron density is estimated to be below 5,000 cm^{-3} for 90% of the time (Němec et al., 2010). Also, the enhanced occurrence rate of detectable nightside ionospheric echoes during solar energetic particle events is consistent with the previous study of Němec et al. (2014). Meanwhile, we do not find any significant enhancement in the local electron density (Figure 3n), which exhibit variable electron densities below ~100 cm^{-3}. We observe significantly enhanced local magnetic fields well above the crustal fields (Figure 3o), implying strong induced fields up to ~40 nT.

As nightside ionospheric traces typically appear as flat, horizontal lines in ionograms (e.g., Diéval et al., 2014; Němec et al., 2010, 2011), it is usually difficult to obtain electron density profiles with dispersion-corrected altitudes on the nightside. However, as exemplified in Figure 4a, some of the ionograms obtained by MARSIS during the Event orbit provide clear ionospheric traces with varying time delays as well as local electron density information, enabling us to perform the inversion routine to correct for the plasma dispersion (Morgan et al., 2008, 2013). Figure 4b shows the electron density profiles with true altitudes successfully corrected for dispersion for three ionograms obtained between the times denoted by the vertical dashed lines in Figures 3i–3p. We see significant difference among the derived profiles in the high-altitude part at >150 km primarily because the shape of the lower-density part is sensitive to the first available point of the ionospheric trace and the local electron density. However, the three profiles converge at lower altitudes <150 km, implying that the primary part of the profile near the peak is relatively well constrained. The dispersion-corrected electron density profiles infer the peak densities of ~1.7 ×10^4 cm^{-3} at altitudes around 120 km at SZA ~140°.

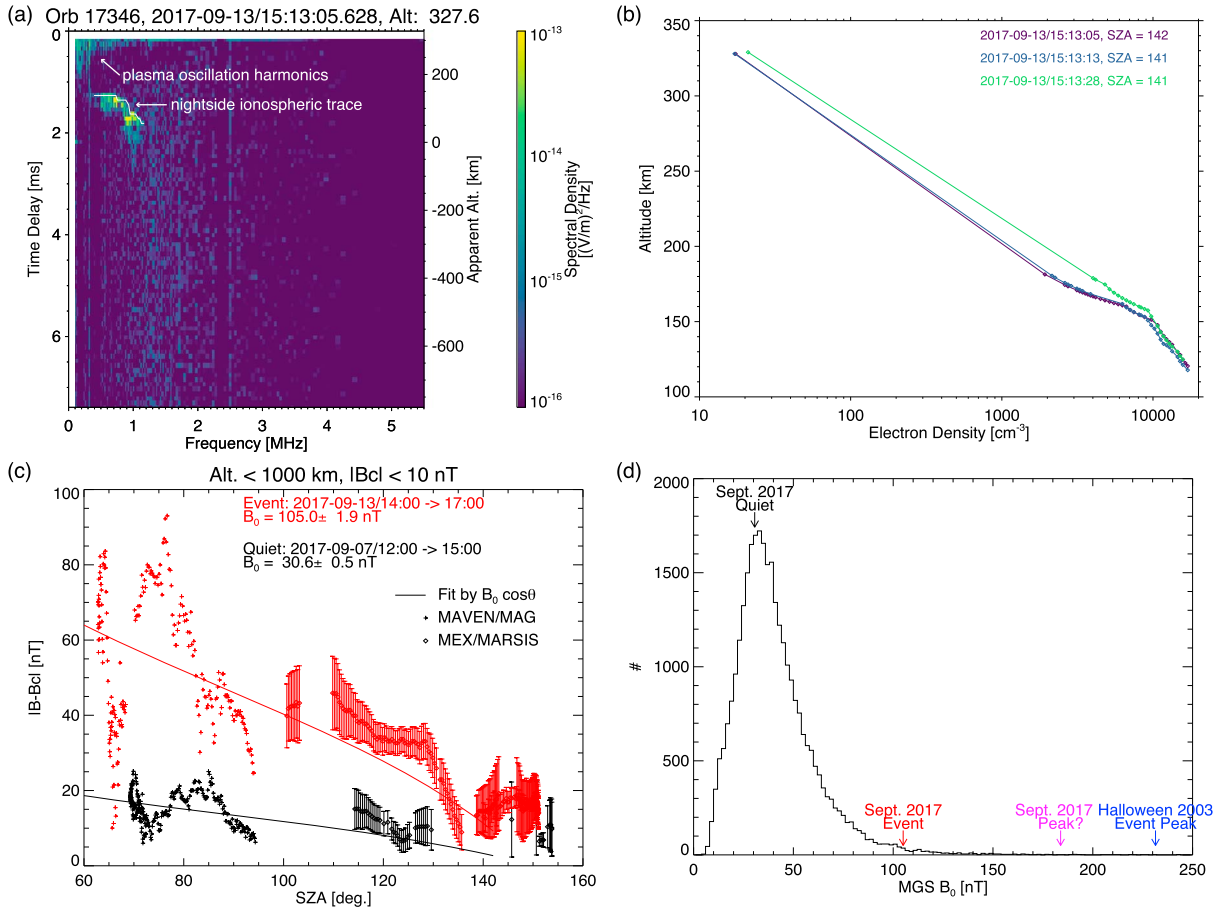

Figure 4. (a) Sample ionogram obtained at 15:13:05 UT during the Event orbit. (b) Nightside electron density profiles as a function of dispersion-corrected altitude during the Event Orbit derived from ionospheric echo traces obtained between the times indicated by the vertical dashed lines in Figures 3i–3p. (c) Induced magnetic field magnitude, $|\mathbf{B}-\mathbf{B}_c|$, as a function of solar zenith angle for the Quiet and Event periods. The diamond symbols indicate $|\mathbf{B}|$ measured by Mars Advanced Radar for Subsurface and Ionosphere Sounding (MARSIS), and the error bars represent the possible range of the induced field magnitude, $|\mathbf{B}|-|\mathbf{B}_c| < |\mathbf{B}-\mathbf{B}_c| < |\mathbf{B}|+|\mathbf{B}_c|$, where $\mathbf{B}_c$ is computed from the spherical harmonic model (Morschhauser et al., 2014). For Mars Atmosphere and Volatile EvolutioN (MAVEN) data points (plus symbols), the computed $\mathbf{B}_c$ is subtracted from the measured $\mathbf{B}$ in a vector fashion. The solid lines in Figure 4c shows fit results by $B_0 \cos\theta$ (Crider et al., 2003), where B_0 is the subsolar magnetic field magnitude and θ is the magnetic pileup boundary normal angle derived from the conic fit by Vignes et al. (2000). (d) Histogram of the subsolar magnetic field magnitude from all the available Mars Global Surveyor (MGS) data at http://sprg.ssl.berkeley.edu/~brain/proxies/subsolfield. MEX = Mars Express; SZA = solar zenith angle; MAG = magnetometer.

These profiles can be compared to Profiles E3, F1, and F2 of Withers et al. (2012) obtained at SZA ~120° during solar energetic particle events, which display comparable peak densities of $\sim 10^4$ cm^{-3} and slightly lower peak altitudes of ~100 km. We note that the capability of obtaining an instantaneous vertical profile of the topside ionospheric density on the deep nightside of Mars, demonstrated for the first time in Figure 4b, is a unique advantage of MARSIS remote measurements as opposed to in situ measurements along oblique orbit tracks and radio occultation measurements with limited SZA ranges.

In summary, the comparison of MARSIS observations during the Event orbit to those during the Quiet orbit indicates (i) disappearance of the ground trace caused by enhanced radio wave absorption at low altitudes, (ii) increase in the peak electron density to $\sim 1-2 \times 10^4$ cm^{-3} at ~120 km altitudes, (iii) no obvious difference in local electron densities at >300 km altitudes, and (iv) enhanced magnetic fields of induced origin up to ~40 nT.

3. Discussion

Here we discuss the source(s) of enhanced ionization in the nightside ionosphere detected by MARSIS during the Event orbit. The nightside ionosphere of Mars is formed by two main sources: plasma transport

from the dayside and local electron impact ionization (Withers, 2009). On one hand, Němec et al. (2010) suggested that plasma transport from the dayside ionosphere provides a primary source for the nightside ionosphere up to SZA of ~125° under normal conditions. On the other hand, significant effects of impact ionization by precipitating suprathermal electrons are predicted and observed below 200 km altitudes (Fillingim et al., 2007, 2010; Fowler et al., 2015; Girazian et al., 2017). We note that the *apparent* peak altitude of ~50 km during the Event orbit (Figure 4a) is much lower than a typical *apparent* peak altitude of 120 km derived from detected nightside echoes (Němec et al., 2010). Though it is uncertain whether the plasma transport limit of SZA ~ 125° holds for disturbed conditions, the primary ionization of the nightside ionosphere during this event is most likely provided by electron impact ionization associated with the intense flux of solar particles, given the low peak density altitudes of ~120 km (Figure 4b). The electron impact ionization around ~120 km altitudes is expected to be caused by >1 keV electrons (Lillis et al., 2009). Furthermore, the disappearance of ground reflection suggests that the bottomside ionosphere is also enhanced, presumably caused by the more energetic part of the solar particle spectrum as demonstrated by numerical models, total electron content measurements, and radio occultations (Lillis et al., 2010; Sheel et al., 2012; Ulusen et al., 2012).

The ionospheric magnetic field measurements on the dayside by MAVEN (Figure 1f) and on the nightside by MARSIS (Figures 3g, and 3o) indicate that the induced magnetic field is enhanced globally in association with the ICME passage. It is known that the dynamic pressure of the upstream solar wind controls the ionospheric magnetic field strength on the dayside (Crider et al., 2003; Harada et al., 2017) and on the nightside (Ferguson et al., 2005). The multipoint measurements by MAVEN and Mars Express suggest that the ionospheric magnetic field enhancement is a truly global phenomenon. Figure 4c shows the induced magnetic field magnitude as a function of SZA from MAG and MARSIS measurements at low altitudes (below 1,000 km) at weak crustal field locations ($|B_c| < 10$ nT), demonstrating the induced magnetic field enhancement over a wide range of SZAs. As vector information cannot be obtained from MARSIS, possible ranges of the induced field magnitude, $|\mathbf{B} - \mathbf{B}_c|$, are shown by the error bars. For each of the Quiet (black) and Event (red) periods, we observe a decreasing trend with increasing SZAs across the terminator as expected from pressure balance on a flaring obstacle surface (Crider et al., 2003), though significant fluctuations are present on top of the overall trend. After Crider et al. (2003), we fit the measured induced field magnitude by $B_0 \cos\theta$, where B_0 is the subsolar magnetic field magnitude and θ is the magnetic pileup boundary normal angle with respect to the Mars-Sun line derived from the conic fit by Vignes et al. (2000). The fit results provide rough estimates of the subsolar field magnitude of $B_0 \sim 31$ nT for the Quiet period and $B_0 \sim 105$ nT for the Event period (Figure 4c). To contextualize these values, Figure 4d shows a histogram of the subsolar magnetic field strength derived from all the available Mars Global Surveyor (MGS) data (Brain et al., 2005) in comparison with the September 2017 solar event as well as the peak B_0 detected by MGS during the Halloween 2003 solar event (e.g., Crider et al., 2005). The Quiet B_0 is found near the peak of the distribution, indicating a typical solar wind condition during the Quiet period. Meanwhile, the Event B_0 is located in the high-B_0 tail of the distribution, and it is in the top 1.1% of the entire MGS B_0 data set. We note that the Event orbit is slightly off the peak of the ionospheric magnetic field magnitude (Figure 1f), and the maximum B_0 during the September 2017 event would be even higher than this. The limited SZA range covered by MAVEN hinders a similar fitting procedure near the peak induced fields, but we nevertheless compute a crude measure of B_0 by simply averaging $|\mathbf{B} - \mathbf{B}_c|/\cos\theta$ measured at $|B_c| < 10$ nT below 1,000 km altitudes at 07:00–08:00 UT on 13 September, resulting in $B_0 \sim 184$ nT (indicated by the magenta arrow in Figure 4d). This implies that the September 2017 solar event can be thought of as a very high dynamic pressure event, although it is not as strong as the Halloween 2003 event (indicated by the blue arrow in Figure 4d).

4. Conclusions

MARSIS measurements of the nightside ionosphere of Mars during the September 2017 solar event along with MAVEN dayside observations reveal that (i) the nightside bottomside ionosphere was significantly enhanced by solar energetic particles as suggested by the disappearance of ground reflection, (ii) the nightside peak electron density was increased to unusually high values of $\sim 1-2 \times 10^4$ cm^{-3} at ~120 km altitudes by enhanced electron impact ionization, and (iii) the induced magnetic field was amplified globally by the high solar wind dynamic pressure during the ICME passage. These measurements provide valuable information for the coordinated effort of the community to understand the global response of the Martian upper atmosphere to the September 2017 solar event.

Acknowledgments
The MARSIS investigation at the University of Iowa was supported by NASA through contract 1560641 with the Jet Propulsion Laboratory. This work was partially supported by the MAVEN project. MARSIS data are available through the Planetary Data System at http://pds-geosciences.wustl.edu. MAVEN data are publicly available through the Planetary Data System at https://pds-ppi.igpp.ucla.edu. The MGS proxy data are available at http://sprg.ssl.berkeley.edu/~brain/proxies/subsolfield.

References

Akalin, F., Morgan, D., Gurnett, D., Kirchner, D., Brain, D., Modolo, R., et al. (2010). Dayside induced magnetic field in the ionosphere of Mars. *Icarus*, *206*(1), 104–111. https://doi.org/10.1016/j.icarus.2009.03.021

Brain, D. A., Halekas, J. S., Lillis, R., Mitchell, D. L., Lin, R. P., & Crider, D. H. (2005). Variability of the altitude of the Martian sheath. *Geophysical Research Letters*, *32*, L18203. https://doi.org/10.1029/2005GL023126

Connerney, J., Espley, J., Lawton, P., Murphy, S., Odom, J., Oliversen, R., & Sheppard, D. (2015). The MAVEN magnetic field investigation. *Space Science Reviews*, *195*(1–4), 257–291. https://doi.org/10. 1007/s11214-015-0169-4

Crider, D. H., Espley, J., Brain, D. A., Mitchell, D. L., Connerney, J. E. P., & Acuña, M. H. (2005). Mars Global Surveyor observations of the Halloween 2003 solar superstorm's encounter with Mars. *Journal of Geophysical Research*, *110*, A09S21. https://doi.org/10.1029/2004JA010881

Crider, D. H., Vignes, D., Krymskii, A. M., Breus, T. K., Ness, N. F., Mitchell, D. L., et al. (2003). A proxy for determining solar wind dynamic pressure at Mars using Mars Global Surveyor data. *Journal of Geophysical Research*, *108*(A12), 1461. https://doi.org/10.1029/2003JA009875

Diéval, C., Morgan, D. D., Němec, F., & Gurnett, D. A. (2014). MARSIS observations of the Martian nightside ionosphere dependence on solar wind conditions. *Journal of Geophysical Research: Space Physics*, *119*, 4077–4093. https://doi.org/10.1002/2014JA019788

Duru, F., Gurnett, D. A., Morgan, D. D., Modolo, R., Nagy, A. F., & Najib, D. (2008). Electron densities in the upper ionosphere of Mars from the excitation of electron plasma oscillations. *Journal of Geophysical Research*, *113*, A07302. https://doi.org/10.1029/2008JA013073

Duru, F., Gurnett, D. A., Morgan, D. D., Winningham, J. D., Frahm, R. A., & Nagy, A. F. (2011). Nightside ionosphere of Mars studied with local electron densities: A general overview and electron density depressions. *Journal of Geophysical Research*, *116*, A10316. https://doi.org/10.1029/2011JA016835

Eparvier, F. G., Chamberlin, P. C., Woods, T. N., & Thiemann, E. M. B. (2015). The solar extreme ultraviolet monitor for MAVEN. *Space Science Reviews*, *195*(1), 293–301. https://doi.org/10.1007/s11214-015-0195-2

Espley, J. R., Farrell, W. M., Brain, D. A., Morgan, D. D., Cantor, B., Plaut, J. J., et al. (2007). Absorption of MARSIS radar signals: Solar energetic particles and the daytime ionosphere. *Geophysical Research Letters*, *34*, L09101. https://doi.org/10.1029/2006GL028829

Ferguson, B. B., Cain, J. C., Crider, D. H., Brain, D. A., & Harnett, E. M. (2005). External fields on the nightside of Mars at Mars Global Surveyor mapping altitudes. *Geophysical Research Letters*, *32*, L16105. https://doi.org/10.1029/2004GL021964

Fillingim, M., Peticolas, L., Lillis, R., Brain, D., Halekas, J., Lummerzheim, D., & Bougher, S. (2010). Localized ionization patches in the nighttime ionosphere of Mars and their electrodynamic consequences. *Icarus*, *206*(1), 112–119. https://doi.org/10.1016/j.icarus.2009.03.005

Fillingim, M. O., Peticolas, L. M., Lillis, R. J., Brain, D. A., Halekas, J. S., Mitchell, D. L., et al. (2007). Model calculations of electron precipitation induced ionization patches on the nightside of Mars. *Geophysical Research Letters*, *34*, L12101. https://doi.org/10.1029/2007GL029986

Fowler, C. M., Andersson, L., Ergun, R. E., Morooka, M., Delory, G., Andrews, D. J., et al. (2015). The first in situ electron temperature and density measurements of the Martian nightside ionosphere. *Geophysical Research Letters*, *42*, 8854–8861. https://doi.org/10.1002/2015GL065267

Girazian, Z., Mahaffy, P., Lillis, R. J., Benna, M., Elrod, M., Fowler, C. M., & Mitchell, D. L. (2017). Ion densities in the nightside ionosphere of Mars: Effects of electron impact ionization. *Geophysical Research Letters*, *44*, 11,248–11,256. https://doi.org/10.1002/2017GL075431

Gurnett, D., Huff, R., Morgan, D., Persoon, A., Averkamp, T., Kirchner, D., et al. (2008). An overview of radar soundings of the Martian ionosphere from the Mars Express spacecraft. *Advances in Space Research*, *41*(9), 1335–1346. https://doi.org/10.1016/j.asr.2007.01.062

Gurnett, D. A., Kirchner, D. L., Huff, R. L., Morgan, D. D., Persoon, A. M., Averkamp, T. F., et al. (2005). Radar soundings of the ionosphere of Mars. *Science*, *310*(5756), 1929–1933. https://doi.org/10.1126/science.1121868

Halekas, J., Taylor, E., Dalton, G., Johnson, G., Curtis, D., McFadden, J., et al. (2015). The solar wind ion analyzer for MAVEN. *Space Science Reviews*, *195*, 125–151. https://doi.org/10.1007/s11214-013-0029-z

Harada, Y., Gurnett, D. A., Kopf, A. J., Halekas, J. S., Ruhunusiri, S., Lee, C. O., et al. (2017). Dynamic response of the Martian ionosphere to an interplanetary shock: Mars Express and MAVEN observations. *Geophysical Research Letters*, *44*, 9116–9123. https://doi.org/10.1002/2017GL074897

Jordan, R., Picardi, G., Plaut, J., Wheeler, K., Kirchner, D., Safaeinili, A., et al. (2009). The Mars express MARSIS sounder instrument. *Planetary and Space Science*, *57*(14–15), 1975–1986. https://doi.org/10.1016/j.pss.2009.09.016

Larson, D. E., Lillis, R. J., Lee, C. O., Dunn, P. A., Hatch, K., Robinson, M., et al. (2015). The MAVEN solar energetic particle investigation. *Space Science Reviews*, *195*(1), 153–172. https://doi.org/10.1007/s11214-015-0218-z

Lee, C. O., Jakosky, B. M., Luhmann, J. G., Brain, D. A., Mays, M. L., Hassler, D. M., et al. (2018). Observations and impacts of the 10 September 2017 solar events at Mars: An overview and synthesis of the initial results. *Geophysical Research Letters*, *45*. https://doi.org/10.1029/2018GL079162

Lillis, R. J., Brain, D. A., England, S. L., Withers, P., Fillingim, M. O., & Safaeinili, A. (2010). Total electron content in the Mars ionosphere: Temporal studies and dependence on solar EUV flux. *Journal of Geophysical Research*, *115*, A11314. https://doi.org/10.1029/2010JA015698

Lillis, R. J., Fillingim, M. O., Peticolas, L. M., Brain, D. A., Lin, R. P., & Bougher, S. W. (2009). Nightside ionosphere of Mars: Modeling the effects of crustal magnetic fields and electron pitch angle distributions on electron impact ionization. *Journal of Geophysical Research*, *114*, E11009. https://doi.org/10.1029/2009JE003379

Morgan, D. D., Diéval, C., Gurnett, D. A., Duru, F., Dubinin, E. M., Fränz, M., et al. (2014). Effects of a strong ICME on the Martian ionosphere as detected by Mars Express and Mars Odyssey. *Journal of Geophysical Research: Space Physics*, *119*, 5891–5908. https://doi.org/10.1002/2013JA019522

Morgan, D. D., Gurnett, D. A., Kirchner, D. L., Fox, J. L., Nielsen, E., & Plaut, J. J. (2008). Variation of the Martian ionospheric electron density from Mars Express radar soundings. *Journal of Geophysical Research*, *113*, A09303. https://doi.org/10.1029/2008JA013313

Morgan, D. D., Gurnett, D. A., Kirchner, D. L., Huff, R. L., Brain, D. A., Boynton, W. V., et al. (2006). Solar control of radar wave absorption by the Martian ionosphere. *Geophysical Research Letters*, *33*, L13202. https://doi.org/10.1029/2006GL026637

Morgan, D. D., Gurnett, D. A., Kirchner, D. L., Winningham, J. D., Frahm, R. A., Brain, D. A., et al. (2010). Radar absorption due to a corotating interaction region encounter with Mars detected by MARSIS. *Icarus*, *206*(1), 95–103. https://doi.org/10.1016/j.icarus.2009.03.008

Morgan, D. D., Witasse, O., Nielsen, E., Gurnett, D. A., Duru, F., & Kirchner, D. L. (2013). The processing of electron density profiles from the Mars Express MARSIS topside sounder. *Radio Science*, *48*, 197–207. https://doi.org/10.1002/rds.20023

Mitchell, D. L., Mazelle, C., Sauvaud, J.-A., Thocaven, J.-J., Rouzaud, J., Fedorov, A., et al. (2016). The MAVEN solar wind electron analyzer. *Space Science Reviews*, *200*(1–4), 495–528. https://doi.org/10.1007/s11214-015-0232-1

Morschhauser, A., Lesur, V., & Grott, M. (2014). A spherical harmonic model of the lithospheric magnetic field of Mars. *Journal of Geophysical Research: Planets*, *119*, 1162–1188. https://doi.org/10.1002/2013JE004555

Němec, F., Morgan, D. D., Diéval, C., & Gurnett, D. A. (2015). Intensity of nightside MARSIS AIS surface reflections and implications for low-altitude ionospheric densities. *Journal of Geophysical Research: Space Physics*, *120*, 3226–3239. https://doi.org/10.1002/2014JA020888

Němec, F., Morgan, D. D., Diéval, C., Gurnett, D. A., & Futaana, Y. (2014). Enhanced ionization of the Martian nightside ionosphere during solar energetic particle events. *Geophysical Research Letters*, *41*, 793–798. https://doi.org/10.1002/2013GL058895

Němec, F., Morgan, D. D., Gurnett, D. A., & Brain, D. A. (2011). Areas of enhanced ionization in the deep nightside ionosphere of Mars. *Journal of Geophysical Research*, *116*, E06006. https://doi.org/10.1029/2011JE003804

Němec, F., Morgan, D. D., Gurnett, D. A., & Duru, F. (2010). Nightside ionosphere of Mars: Radar soundings by the Mars Express spacecraft. *Journal of Geophysical Research*, *115*, E12009. https://doi.org/10.1029/2010JE003663

Nielsen, E., Morgan, D., Kirchner, D., Plaut, J., & Picardi, G. (2007). Absorption and reflection of radio waves in the Martian ionosphere. *Planetary and Space Science*, *55*(7–8), 864–870. https://doi.org/10.1016/j.pss.2006.10.005

Sheel, V., Haider, S. A., Withers, P., Kozarev, K., Jun, I., Kang, S., et al. (2012). Numerical simulation of the effects of a solar energetic particle event on the ionosphere of Mars. *Journal of Geophysical Research*, *117*, A05312. https://doi.org/10.1029/2011JA017455

Trotignon, J., Mazelle, C., Bertucci, C., & Acuña, M. (2006). Martian shock and magnetic pile-up boundary positions and shapes determined from the Phobos 2 and Mars Global Surveyor data sets. *Planetary and Space Science*, *54*(4), 357–369. https://doi.org/10.1016/j.pss.2006.01.003

Ulusen, D., Brain, D. A., Luhmann, J. G., & Mitchell, D. L. (2012). Investigation of Mars' ionospheric response to solar energetic particle events. *Journal of Geophysical Research*, *117*, A12306. https://doi.org/10.1029/2012JA017671

Vignes, D., Mazelle, C., Rme, H., Acuña, M. H., Connerney, J. E. P., Lin, R. P., et al. (2000). The solar wind interaction with Mars: Locations and shapes of the bow shock and the magnetic pile-up boundary from the observations of the MAG/ER Experiment onboard Mars Global Surveyor. *Geophysical Research Letters*, *27*(1), 49–52. https://doi.org/10.1029/1999GL010703

Withers, P. (2009). A review of observed variability in the dayside ionosphere of Mars. *Advances in Space Research*, *44*(3), 277–307. https://doi.org/10.1016/j.asr.2009.04.027

Withers, P., Fillingim, M. O., Lillis, R. J., Häusler, B., Hinson, D. P., Tyler, G. L., et al. (2012). Observations of the nightside ionosphere of Mars by the Mars Express Radio Science Experiment (MaRS). *Journal of Geophysical Research*, *117*, A12307. https://doi.org/10.1029/2012JA018185